HHS Public Access

Author manuscript

Hepatology. Author manuscript; available in PMC 2020 October 01.

Published in final edited form as:

Hepatology. 2019 October ; 70(4): 1168–1184. doi:10.1002/hep.30669.

Impaired chylomicron assembly modifies hepatic metabolism through bile acid dependent and transmissible microbial adaptations

Yan Xie[1], **Hitoshi Matsumoto**[1], **Susan Kennedy**[1], **Elizabeth P. Newberry**[1], **William Moritz**[1], **Brian J. DeBosch**[2], **Kelle H. Moley**[3], **Deborah C. Rubin**[1], **Brad W. Warner**[4], **Andrew L. Kau**[1], **Phillip I. Tarr**[2], **Todd N. Wylie**[2,5], **Kristine M. Wylie**[2,5], **Nicholas O. Davidson**[1,6]

[1]Department of Medicine, Washington University School of Medicine, St. Louis, MO 63110, USA

[2]Department of Pediatrics, Washington University School of Medicine, St. Louis, MO 63110, USA

[3]Department of Obstetrics and Gynecology, Washington University School of Medicine, St. Louis, MO 63110, USA

[4]Department of Surgery, Washington University School of Medicine, St. Louis, MO 63110, USA

[5]Department of McDonnell Genome Institute, Washington University School of Medicine, St. Louis, MO 63110, USA

[6]Lead contact

Abstract

The mechanisms by which alterations in intestinal bile acid (BA) metabolism improve systemic glucose tolerance and hepatic metabolic homeostasis are incompletely understood. Here we examined metabolic adaptations in mice with conditional intestinal deletion of the abetalipoproteinemia (ABL) gene microsomal triglyceride transfer protein (*Mttp-IKO*), which blocks chylomicron assembly and impairs intestinal lipid transport. *Mttp-IKO* mice exhibit improved hepatic glucose metabolism and augmented insulin signaling, without weight loss. These adaptations included decreased BA excretion, increased pool size, altered BA composition and increased Fgf15 production. *Mttp-IKO* mice absorb fructose normally, but are protected against dietary fructose-induced hepatic steatosis, without weight loss or changes in energy expenditure. In addition, *Mttp-IKO* mice exhibit altered cecal microbial communities, both at baseline and also following fructose feeding, including increased abundance of *Bacteroides* and *Lactobacillus* genera. Transplantation of cecal microbiota from chow-fed *Mttp-IKO* mice into antibiotic-treated wild-type recipients conferred transmissible protection against fructose-induced hepatic steatosis in association with a bloom in *Akkermansia* and increased *Clostridium* XIVa genera, whose abundance was positively correlated with fecal coprostanol and total neutral sterol

Correspondence: nod@wustl.edu.

AUTHOR CONTRIBUTIONS

YX, HM, SK, EPN, BJD, KHM, were involved in the design of physiological and molecular phenotyping experiments, performed studies and participated in data interpretation; WM, DCR, BWW, ALK, PIT, TNW, KMW were involved in experimental design and data interpretation of experiments concerning microbial profiling and in the writing of the manuscript; NOD was involved in the design and interpretation of all the experiments and in drafting the manuscript. The authors acknowledge with deep gratitude the editorial assistance of Anastasia E. Zylka.

excretion in recipient mice. However, antibiotic treated *Mttp-IKO* mice were still protected against fructose induced hepatic steatosis, suggesting that changes in microbiota are not required for this phenotype. Nevertheless, we found increased abundance of fecal *Akkermansia* from two adult ABL subjects with *MTTP* mutations, compared to their heterozygous parents and within the range noted in six healthy control subjects. Furthermore, *Akkermansia* abundance across all subjects was positively correlated with fecal coprostanol excretion.

Conclusion: The findings collectively suggest multiple adaptive pathways of metabolic regulation following blocked chylomicron assembly, including shifts in BA signaling and altered microbial composition that confer a transmissible phenotype.

Keywords

chylomicrons; abetalipoproteinemia; *Akkermansia*; bile acids; FGF15/19

INTRODUCTION

The global pandemic of obesity and its metabolic sequelae (1) have fueled interest in the mechanisms by which targeted interventions might yield a durable therapeutic response (2). Among bariatric procedures both Roux-en-Y gastric bypass (RGBP) and vertical sleeve gastroplasty (VSG) induce sustained weight loss through mechanisms including alterations in satiety, delivery of nutrients to the distal intestine, bypass of pancreatico-biliary digestive enzymes and altered secretion of foregut peptides (3–5). Other postulated mechanisms are linked to changes in enterohepatic cycling of bile acids (BA) and altered gut microbiota, which alter the size and composition of the recycling BA pool (6–8). Specifically, changes following VSG include altered BA signaling via the farnesoid X receptor (FXR) and downstream targets including fibroblast growth factor 15/19 (FGF15/19) and TGR5/GPBAR-1. These effectors produce favorable shifts in glucose and lipid metabolism and amelioration of hepatic steatosis and other indices of nonalcoholic fatty liver disease (NAFLD) (8, 9). Many of the changes invoked by VSG and RGBP were replicated in mice following surgical diversion of bile directly into the ileum (7).

Human and mouse data support a key regulatory role of BAs in hepatic glucose and lipid metabolism, because BA sequestrants—used as cholesterol lowering drugs—favorably alter obesity and glucose metabolism (10, 11). Other studies showed that intestinal FXR agonist administration augmented TGR5 signaling to improve hepatic metabolism (12), findings that support an emerging consensus that bile acid pathways may be druggable targets for metabolic disorders (13). The finding that inhibition of ileal BA uptake was protective against NAFLD in mice (14) raised the additional possibility that perturbations in enterocyte fat trafficking might signal systemic adaptations in lipid and glucose metabolism.

Here we show that mice with conditional intestinal deletion of microsomal triglyceride transfer protein (*Mttp-IKO*), in which chylomicron assembly and intestinal lipid export are impaired (15), also exhibit altered enterohepatic signaling via FXR and LXR pathways as well as alterations in BA composition and cycling. In addition, we observed shifts in cecal microbial taxa in *Mttp-IKO* mice, including the transmissible protection against fructose-induced hepatic steatosis in wild-type recipients. Our findings suggest a complex range of

metabolic adaptations to impaired intestinal lipid absorption, some of which were observed in subjects with *MTTP* mutations and abetalipoproteinemia (16).

METHODS.

Animals:

All experiments were in accordance with institutional guidelines (IACUC #20150284). $Mttp^{f/f}$ Villin Cre ER^{T2} mice (15) were studied at 12–14 weeks unless otherwise noted. Littermate controls were used in all experiments.

Metabolic studies, fructose feeding and cecal transplants:

Mice (group-housed by genotype) were fed either a 60% fructose diet (Teklad #TD89247) or 20% fructose supplemented water where indicated. For cecal microbiota transplantation, conventionally housed C57BL/6J wild type mice (Jax) were treated with antibiotics (17). Cecal slurries or monocolonization extracts were administered by oral gavage for 3 consecutive days and then alternate days (up to 10days). Glucose tolerance, fructose absorption, Oxymax studies, BA pool size and species, primers for Q-RT-PCR, cell extracts and immunological detection are detailed in Supplemental Methods.

Human Studies.

Two separate families with abetalipoproteinemia were studied as approved by the human studies committee of Washington University School of Medicine (IRB#201203104). Family 1 (18), includes a 35yr F proband (homozygous G865X) and her 61 yr F parent (heterozygous G865X). Family 2 includes a 22 yr M proband (compound heterozygous Intron 13+1, G>A; A667 fs X36) and his heterozygous parents (mother 50, heterozygous Intron 13+1 G>A; father 48, heterozygous A677A fs X36). In addition, we recruited 6 normal, healthy adult subjects (Supplemental Methods) undergoing routine outpatient screening colonoscopy. No subject was taking lipid lowering or diabetes medication and none had taken antibiotics in the preceding 6 months.

16S rRNA gene sequencing.

Bacterial DNA was extracted (19), 16S rRNA gene V4 region sequenced for operational taxonomic unit (OTUs) assignment and classification as detailed in Supplemental Methods.

Statistics:

Data were analyzed using GraphPad Prism 7.02 by unpaired t-test or Mann-Whitney test. For multigroup comparisons, statistical differences were performed by one-way ANOVA and Tukey's multiple comparison post-hoc test. The level of significance was set at $p<0.05$ and indicated using *$p<0.05$; **$p<0.01$.

RESULTS

Hepatic insulin signaling is improved, hepatic gluconeogenesis and intestinal glucose transport are decreased in chow-fed *Mttp-IKO* mice:

Mttp-IKO mice fed a low fat chow diet exhibit improved glucose tolerance both with oral (Figure 1A, left) and intraperitoneal challenge (Figure 1A, right) and without changes in energy expenditure (Supplemental Figure S1 A–D). In addition, *Mttp-IKO* mice exhibit decreased hepatic gluconeogenesis with increased glycogen content (Figure 1B) and an impaired response to pyruvate challenge (Supplemental Figure S1, E), yet exhibit a normal response to glucagon administration (Figure 1C), suggesting intact cAMP signaling (20). Hepatic insulin signaling was also enhanced in *Mttp-IKO* mice as evidenced by decreased nuclear FoxO1 expression (Figure 1D, Supplemental Figure S1F), and increased expression of Irs1 and its downstream targets including phospho-Akt and phospho-Gsk3β(21) (Figure 1E). These changes were accompanied by decreased intestinal glucose transport (Figure 1F, left) and decreased expression of both Sglt-1 (Figure 1F, middle) and the facilitative glucose transporter Glut2 (22) (Figure 1F, right).

Mttp-IKO mice absorb intestinal fructose normally and are protected against fructose-induced glucose intolerance and hepatic steatosis:

Despite impaired intestinal glucose absorption, *Mttp-IKO* mice exhibit comparable fructose uptake and disappearance (Figure 2A, left), with comparable expression of the facilitative fructose transporter Glut5 (Figure 2A, right). Because *Mttp-IKO* mice exhibit reduced hepatic lipid content despite increased expression of lipogenic and cholesterogenic genes (Supplemental Figure S2A–C), as previously noted (15), we fed mice of both genotypes a fructose-supplemented diet and determined the impact on hepatic steatosis. *Mttp-IKO* mice again exhibited improved glucose tolerance (Figure 2B), along with reduced hepatic steatosis (Figure 2C, left) and, as in chow-fed mice, increased lipogenic gene expression (Acc, Fasn) as well as increased cholesterogenic genes including Srebp2 and Hmgcr (Figure 2C, right). *Mttp-IKO* mouse livers showed increased expression of the LXR target genes Abcg5/8 as well as the ChREBP target Fgf21 and decreased expression of Cyp7a1 mRNA with increased expression of Shp, Fgfr4 mRNAs (Figure 2 C, right). We then asked if inducible deletion of intestinal *Mttp* might reverse the glucose intolerance observed in control (Mttp f/f Villin Cre ER^{T2}) mice. Accordingly, mice were fed a fructose rich diet for ~18 weeks and then studied ~5 weeks after TAM administration (ie 23 weeks). Those studies revealed improved glucose tolerance following intestinal *Mttp* deletion (Figure 2D), along with decreased hepatic steatosis and induction of many of the aforementioned mRNAs including Abcg5/8, Hmgcr and Fgf21 (Figure 2E). As noted in chow fed mice, there was no change in energy expenditure over the period of fructose feeding (Supplemental Figure S2D–G). These findings, suggest that adaptive mechanisms—independent of fructose absorption or weight loss—improve the systemic metabolic profile in fructose-fed *Mttp-IKO* mice, potentially including a combination of LXR- and FXR-dependent pathways.

Mttp-IKO mice exhibit altered enterohepatic BA cycling, composition and increased intestinal Fgf15 production:

Hepatic expression of BA synthetic mRNAs in chow fed *Mttp-IKO* mice revealed upregulated Shp and downregulated Cyp7a1, Cyp7b1 and Cyp8b1 (Figure 3A), in association with decreased fecal BA excretion (Fig 3B, left), increased BA pool size (Figure 3B, right) and a shift of the pool into proximal small intestinal segments, P2, 4, 6 (Figure 3C, right). The decreased expression of Cyp7b1 may reflect the increased accumulation of hepatic oxysterol previously observed in *Mttp-IKO* mice (23). There was also a shift in BA species distribution in liver and ileum (Figure 3D) as well as in serum and feces (Supplemental Figure S3 A, B) with increased abundance of tauromuricholate and taurocholate in livers from *Mttp-IKO* mice and decreased abundance of ursodeoxycholate, cholate, chenodeoxycholate and deoxycholate in ileum of *Mttp-IKO* mice. The net effect of these shifts in BA species tended to increase the ratio of FXR antagonists to FXR agonists (24, 25) in the liver, ileum and serum (Supplemental Figure S3C) and also decreased the proportion of 12α-hydroxylated BA species (26) (Supplemental Figure S3D), a change previously associated with improved metabolic homeostasis. Those observations imply a net FXR *antagonism* in *Mttp-IKO* mice, consistent with decreased ileal expression of the FXR target Tgr5 (Figure 3E). We observed increased Fgf15 protein abundance in ileal and jejunal mucosa (Figure 3F), along with increased serum Fgf15 (Figure 3F), which together suggest increased intestinal Fgf15 production, in *Mttp-IKO* mice. These changes in Fgf15 occurred without alteration in ileal FXR mRNA abundance and with decreased expression of both RXRα (27) and Diet1 (28) mRNAs. However, we observed decreased ileal mRNA abundance (Figure 3E) and protein expression (Supplemental Figure S3F) of the transcriptional repressor Klf15, which has been previously implicated in the circadian control of BA metabolism (29). BA deconjugation was also decreased in liver, ileum and feces of *Mttp-IKO* mice (Supplemental Figure 3E). Considered together, these findings suggest that simultaneous changes in enterohepatic BA cycling along with regional shifts in intestinal BA distribution and species may play a role in the metabolic adaptations observed in chow fed *Mttp-IKO* mice, and that the mechanisms involve both selective FXR activation and inhibition.

Further evidence to support altered enterokine signaling in *Mttp-IKO* mice include increased fasting and post-prandial GLP-1 and GIP levels as well as decreased gastric emptying (Supplemental Figures S4 A–C). In addition, TGR5 mRNA abundance was increased in total liver (Figure 3A) and brown adipose tissue of *Mttp-IKO* mice, (Supplemental Figure S4D) but decreased in jejunum (Supplemental Figure S4D) and ileum (Figure 3E) and unchanged in colon, muscle and white adipose tissue (Supplemental Figure S4D). We also demonstrated increased mRNA abundance of the long chain fatty acid (LCFA) receptor Gpr120 mRNA in proximal intestine of *Mttp-IKO* mice (Supplemental Figure S4E) which suggests a possible LCFA dependent pathway for GIP and GLP-1 secretion (30).

Protection against hepatic steatosis in *Mttp-IKO* mice is associated with increased fecal neutral sterol excretion and altered microbial taxa:

To further pursue the dynamic changes in the adaptive response to fructose feeding, we undertook a short-term (10 day) challenge with dietary fructose. *Mttp-IKO* mice

demonstrated reduced hepatic steatosis (Figure 4A, left), but no changes by genotype in hepatic Cyp7a1, Cyp8b1 or Shp mRNA expression (Figure 4A, right). By contrast, mRNAs encoding sterol regulated metabolic pathways (Srebp2, Hmgcr, Abcg5, Abca1) were upregulated in *Mttp-IKO* mice (Figure 4A, right) along with increased fecal neutral sterol excretion (including the bacteria-derived cholesterol degradation products coprostanol and cholestanone, Figure 4 B, left) and decreased mRNA expression of intestinal cholesterol transporter genes (Figure 4 B, right). We also asked if changes in the abundance of cecal short chain fatty acids (SCFA) might explain the metabolic adaptations observed in *Mttp-IKO* mice, as recently suggested in other mouse models of altered metabolic homeostasis (31). However, we found *reduced* levels of total SCFA including acetate and butyrate in cecal extracts from chow fed *Mttp-IKO* mice (Figure 4C, left), implying reduced bacterial carbohydrate breakdown and fermentative activity. Additionally, fructose feeding further reduced total and individual cecal SCFA abundance with no differences by genotype (Figure 4C, right), making it unlikely that increased SCFA production contributes to the metabolic adaptations observed by genotype. In line with that suggestion, mRNA abundance for the SCFA receptor Gpr41 was decreased in *Mttp-IKO* mice (Supplemental Figure S4F).

Because alterations in gut microbes influence components of intestinal lipid, BA and cholesterol metabolism (32), we next examined the effects of blocked chylomicron assembly on cecal bacterial communities, comparing amplicons generated (Methods) from cohoused (by genotype and diet) control and *Mttp-IKO* mice. The overall bacterial abundance (Methods) was no different by genotype and increased following fructose feeding (Supplemental Figure S5A), while overall Shannon diversity and richness of the bacterial community was indistinguishable by genotype and decreased with fructose feeding. (Supplemental Figure S5 B, C). We clustered an average of 24557 reads per sample (range 16619–29777) to OTUs. After rarefying to 16270 reads per samples and removing OTUs with less than 5 reads, we identified 886 distinct OTUs. These communities contained six major phyla, (Figure 4D) with changes including increased abundance of Bacteroidetes and decreased Firmicutes in chow fed *Mttp-IKO* mice, (Figure 4D), which was confirmed by linear discriminant analysis for effect size [LEfSe, Methods, Supplemental Figure S5 D, E)

Fructose feeding reduced the relative abundance of Firmicutes and increased the relative abundance of Bacteroidetes in control mice, but not in *Mttp-IKO* mice (Figure 4D and Supplemental Figure S5 F, G). Further analysis at the genus level (Supplemental Methods) demonstrated expansion of *Bacteroidetes_unclassified* and *Lactobacillus* genera in chow fed *Mttp-IKO* mice with further relative expansion of *Bacteroides* following fructose feeding (Figure 4E left panel, Supplemental Figure S6A). Principal coordinates analysis (PCoA, Methods) segregated cecal communities by both diet and genotype (Figure 4F). LEfSe also identified signature genera either by genotype or diet. For the genotype effects (same diet), genus-level abundance of *Bacteroides*, *Lactobacillus* and *Porphyromonodaceae _unclassified* were increased in chow fed *Mttp-IKO* mice (Supplemental Figure S6B), while *Lactobacillus and Lachnospiraceae_unclassified* were increased with fructose feeding (Supplemental Figure S6C). For the fructose diet effects within the same genotype, genus-level abundance of *Bacteroides,* and *Alistipes* were increased in fructose fed mice of both genotypes (Supplemental Figure S6 D, E).

Increased fecal neutral sterol excretion and attenuated hepatic steatosis in *Mttp-IKO* mice are associated with alterations in defined microbial taxa:

We next sought to refine some of the functional associations noted between the improved metabolic profile in *Mttp-IKO* mice—specifically the decreased hepatic steatosis and increased fecal sterol loss—with changes in microbial taxa (Supplemental Table S1). Of note, the relative abundance of genus *Lactobacillus* (phylum Firmicutes) was significantly associated with reduced hepatic triglyceride, total cholesterol and free cholesterol content (Figure 5A, left, middle and right), and with increased fecal cholestanone (Figure 5B, left) and total neutral sterol excretion (Figure 5B, right). Similarly, the relative abundance of *Clostridium XIVa* was significantly associated with decreased hepatic triglyceride content (Figure 5C, left) and increased total fecal neutral sterol excretion (Figure 5C, right). By contrast, the relative abundance of *Alistipes* was positively correlated with increased hepatic TG and decreased fecal coprostanol (Figure 5D).

A transmissible phenotype of increased fecal neutral sterol excretion and attenuated hepatic steatosis in wild-type mice associated with alterations in defined microbial taxa, including *Akkermansia Muciniphila*:

Antibiotic treatment of control and *Mttp-IKO* mice reduced cecal bacterial load (Supplemental Figure S7A) but the protection phenotype following fructose feeding was fully preserved in *Mttp-IKO* mice (Supplemental Figure S7B). Antibiotic treated *Mttp-IKO* mice still demonstrated decreased hepatic Cyp7a1 and increased Fasn mRNAs (Supplemental Figure S7C) with decreased Cyp7a1 activity as evidenced by serum C4 levels (Supplemental Figure S7D), suggesting that changes in microbial taxa are not required for the metabolic adaptations described. Recognizing this caveat, we persisted in trying to understand how alterations in microbial taxa might potentially modify the metabolic adaptations following fructose feeding. Accordingly, we undertook microbial transplantation of cecal contents from chow fed control (CCC) or *Mttp-IKO* mice (MCC) into antibiotic treated (Supplemental Methods) wild-type (WT) recipient mice (cohoused by donor cecal genotype) and fed them a high fructose diet. WT mice receiving MCC exhibited reduced hepatic triglyceride and cholesterol content (Figure 6A, left) and analysis of hepatic mRNAs recapitulated some of the adaptive changes (decreased Cyp7a1, increased Fasn, Figure 6A, right) noted in chow-fed *Mttp-IKO* mice (compare Figure 3A and Supplemental Figure S2B). Furthermore, we observed increased fecal cholesterol, coprostanol, cholestanone and total neutral sterol output in mice receiving MCC (Figure 6B, left) along with decreased expression of intestinal cholesterol transporter mRNAs Npc1l1 and Abca1 expression (Figure 6B, right) in those mice. In addition, we observed increased ileal Fgf15 expression in mice receiving MCC (Figure 6C). Those findings together suggest that cecal microbial communities from chow fed *Mttp-IKO* mice impart a transmissible metabolic phenotype when introduced into fructose fed WT recipients.

Phylum level changes in the cecal microbial communities of transplanted mice included decreased Firmicutes in mice receiving cecal contents from *Mttp-IKO* mice (MCC) coupled with a major expansion of Verrucomicrobia (Figure 6D). We found no change in overall cecal bacterial load (Supplemental Figure S8A) but observed decreased Shannon diversity and richness in MCC treated mice (Supplemental Figure S8 B, C). Genus level changes

observed in MCC treated mice include a bloom in *Akkermansia*, increased abundance of *Parabacteroides* and *Clostridium XIVa* and decreased abundance of *Lachnospiraceae_unclassified* (Figure 6E and Supplemental Figure S8D), which together account for the phylum level changes noted in MCC treated mice. PCoA revealed separation of cecal communities by both donor (D) and recipient (R) genotype (Figure 6F), suggesting an important role of both diet and donor genotype in the distribution of microbial taxa in WT recipients following fructose feeding.

We next ascertained the functional impact of those changes in microbial communities. Relative abundance of *Akkermansia* was correlated with decreased hepatic free cholesterol content and increased fecal neutral sterol and coprostanol excretion (Figure 7A, left, middle, right). Those findings were confirmed when we quantitated *Akkermansia* copy number, with greater absolute *Akkermansia* abundance in MCC versus CCC animals (Supplemental Figure S9A). *Akkermansia* abundance was also associated with increased fecal total neutral sterol, cholesterol, cholestanone and coprostanol excretion (Supplemental Figure S9 B–E) and reduced hepatic triglyceride and cholesterol content (Supplemental Figure S9 F,G). *Clostridium_XIVa* abundance was correlated with decreased hepatic cholesterol content (Figure 7B, left) and with increased fecal neutral sterol and coprostanol excretion (Figure 7B, middle, right,). We also demonstrated correlations with less favorable metabolic phenotypes (Supplemental Table 2), including increased relative abundance of *Alistipes* with decreased fecal neutral sterol and cholestanone (Figure 7D, left, right) and increased relative abundance of *Mucispirillum* with hepatic free cholesterol content (Figure 7C, left) and with decreased fecal neutral sterol and coprostanol excretion, respectively (Figure 7C, middle, right). However, *Akkermansia muciniphila* monocolonization failed to reduce hepatic lipid content in antibiotic treated, fructose fed WT mice (despite increasing fecal cholesterol excretion) and we found no change in *Akkermansia* abundance between treated and control groups (Supplemental Figure S10A–C).

Akkermansia is enriched in Abetalipoproteinemia patients and positively correlated with fecal coprostanol excretion.

We examined fecal microbial taxa in 5 subjects, from two abetalipoproteinemia (ABL) families, where two probands exhibit absent MTTP in both liver and small intestine. We generated 73895 to 131546 reads per sample from which 2116 OTUs were identified and assigned taxonomically into 7 phyla and 110 genera (Supplemental Figure S11 A, B). Gut microbial communities from the ABL probands clustered distinctly from their heterozygous parents, shown by PCoA analysis of weighted UniFrac distance (Figure 8A). The relative *Akkermansia* abundance was increased in ABL probands compared to their heterozygous parents (Supplemental Figure S11B), with higher absolute *Akkermansia* content in ABL probands compared to their heterozygous parents (Figure 8B). Finally, even though absolute fecal *Akkermansia* content was within the range found in six healthy control subjects (Figure 8B), we observed across the group that fecal *Akkermansia* abundance was positively correlated with fecal coprostanol excretion, similar to what we observed in the cecal microbial transfer experiments.

DISCUSSION

Here we define a complex signaling network that improves metabolic homeostasis following inhibition of chylomicron assembly and blocked enterocyte lipid export and in advance of weight loss (Supplemental Figure S12). *Mttp-IKO* mice phenocopy the intestinal manifestations observed in ABL subjects (15, 16, 23). Among the key adaptations are increased cholesterol efflux, reflecting both decreased enterocyte uptake and increased hepatobiliary cholesterol secretion (15, 23), which together result in increased fecal neutral sterol excretion (Supplemental Figure S12). The current work details additional changes in both intestinal and hepatic glucose metabolism and also a marked reduction in fructose-induced hepatic steatosis, even though fructose absorption was unchanged. The basis for these metabolic adaptations at least partly reflects altered BA signaling and shifts in microbial taxa (Supplemental Figure S12), as evidenced by a transmissible phenotype when examined in wild-type recipient hosts, including a bloom in *Akkermansia*. We also observed increased abundance of fecal *Akkermansia* in two ABL probands compared to their heterozygous parents.

The rapid improvement of glucose intolerance in advance of detectable weight loss is a feature of several bariatric procedures (4, 8) and suggests that fat malabsorption *per se* is not the primary mechanism driving this metabolic shift. This conclusion is supported by our earlier (15, 23) and current observations in which we found no weight loss in *Mttp-IKO* mice over the time course (3–5 weeks) of these studies. We observed decreased intestinal glucose uptake, yet no change in intestinal fructose absorption in *Mttp-IKO* mice. Based on those findings, coupled with earlier observations that hepatic lipogenesis was increased in chow fed *Mttp-IKO* mice (15), we predicted that those mice would exhibit exaggerated hepatic steatosis when challenged with dietary fructose. However, that was not the case. Instead, we found that fructose-fed *Mttp-IKO* mice were protected against hepatic steatosis despite further induction of lipogenic and cholesterogenic genes.

Several features of these metabolic adaptations reflect shifts in enterohepatic BA cycling and signaling, including changes that recapitulate some of the adaptations observed with bariatric interventions such as VSG. This response suggests on the one hand a role for FXR-dependent signaling in mediating improved glucose tolerance (8). On the other hand, contrasting effects were observed with ileal bile diversion (7), where FXR antagonism was implicated (increased hepatic Cyp7a1 mRNA in association with increased TβMCA). Other work showed the gut specific FXR agonist fexeramine improved glucose tolerance and mitigated several obesity-associated metabolic complications (33). *Mttp-IKO* mice demonstrated an expanded BA pool with redistribution into the small intestine and decreased fecal BA excretion (Supplemental Figure S12), changes similar to those observed in high fat fed mice treated with tempol (34), where increased TβMCA abundance and shifts in BA composition promote FXR antagonism. To further complicate matters, we found increased intestinal Fgf15 expression in *Mttp-IKO* mice along with decreased hepatic Cyp7a1, findings divergent from those following VSG, ileal bile diversion or tempol treatment (7, 9, 34), where Fgf15 was decreased and Cyp7a1 increased. These apparently conflicting observations highlight a conundrum with respect to the role of FXR signaling pathways in the context of metabolic adaptation and weight loss, since both FXR agonists (gain-of-

function) [Reviewed in (13)] and loss-of-function/FXR antagonists (35) offer metabolic benefits depending on the circumstances. We also observed increased FNS excretion in *Mttp-IKO* mice as well as in WT mice receiving cecal microbiota from those mice, along with decreased expression of intestinal cholesterol transporters and increased expression of cholesterol efflux genes. The mechanisms underlying the biliary cholesterol secretion in *Mttp-IKO* mice likely include augmented LXR signaling, mediated through a combination of increased hepatic oxysterol content as previously noted (23) as well as via Fgf 15 mediated activation of LXR (36). The increased intestinal cholesterol efflux in *Mttp-IKO* mice might conceivably include both transintestinal pathways (37) as well as augmented apical efflux. Further study will be required to resolve those possibilities.

Another element of the metabolic adaptations observed concerns the shifts in microbial taxa with blocked chylomicron assembly. Because high fat feeding in mice tends to increase the relative abundance of Firmicutes and decreases that of Bacteroidetes (38), we predicted that the microbiome of chow-fed *Mttp-IKO* mice would likewise be enriched in Firmicutes with reduced abundance of Bacteroidetes, because of the presence of fat malabsorption. However, we also recalled findings showing increased Bacteroidetes and decreased Firmicutes abundance as adaptive changes in high fat fed mice subjected to either ileal diversion (7) or gastric bypass surgery (39), with both interventions producing metabolic adaptations (and changes in Bacteroidetes:Firmicutes ratio) similar to those seen here. Our findings suggest that the metabolic shifts in enterohepatic BA cycling, pool size and species distribution are likely to be primary factors driving the phenotypes observed following blocked chylomicron assembly. Furthermore, we demonstrated a transmissible component to the protection against fructose-induced hepatic steatosis in which the abundance of certain taxa was correlated with important adaptive pathways leading to metabolic improvement. These include the association of increased relative abundance of *Akkermansia* and *Clostridium-XIVa* genera with increased fecal neutral sterol excretion and reduced hepatic lipid content. The findings in regard to the bloom in *Akkermansia* observed following microbial transfer from cecal contents of *Mttp-IKO* mice into antibiotic treated wild-type recipients resemble other findings suggesting an adaptive role for *Akkermansia* in protection against high fat diet induced obesity (40, 41). Other recent work in mice has shown that bile diversion to the ileum improves glucose homeostasis via FXR-Glp-1 signaling in conjunction with increased abundance of *Akkermansia (42)* The implications from those preclinical studies are in line with observations in overweight and obese human subjects undergoing calorie restriction where enrichment in *Akkermansia* was associated with healthier metabolic status (43).

Those findings notwithstanding, our studies in antibiotic treated mice imply that changes in the microbiota are not a *required* component of the protection phenotype observed in fructose fed *Mttp-IKO* mice. But here again, caution is warranted. Our antibiotic treatment lasted only for the 10day period of fructose feeding, while in other reports, mice were treated for 4 weeks (12) during which body weight tended to decrease (which would complicate the interpretation of our studies). Further studies showed that treatment with polymyxin B and neomycin markedly reduced fructose induced hepatic steatosis (44). Yet other studies showed that germ-free mice fail to develop fructose induced hepatic steatosis (45), findings in keeping with the reduced hepatic steatosis noted in toll-like receptor 4 mutant C3H/HeJ mice (46). Taken together, the findings suggest an important (even if not

required) contribution of host microbial taxa to fructose induced hepatic steatosis in C57BL6 mice.

Another element is that monocolonization of antibiotic treated WT mice with *Akkermansia mucinophila* failed to replicate the findings in WT mice treated with cecal communities from *Mttp-IKO* mice. We employed a monocolonization regimen of alternate day (for 10days) administration of *A. mucinophila* in order to replicate the approach used in the cecal microbial transfer experiments. Other investigators who reported monocolonization experiments employed a daily regimen for 4 weeks in high fat fed mice (40, 41). It is worth noting that we did not find enrichment in cecal *Akkermansia* in treated mice, suggesting those mice were not colonized under the conditions tested (ie high fructose, low fat). As above, we acknowledge that a daily and more prolonged monocolonization approach might yield different results, but it is equally possible that other taxa are required to promote *Akkermansia* colonization.

The underlying mechanisms and the signaling pathways involved in restoring impaired hepatic lipid metabolism is of relevance to a broader understanding of pathways promoting NAFLD in humans (47). Finally, the findings suggest that non-invasive approaches to mediating these adaptations in subjects with progressive forms of NAFLD, for example by interrupting intestinal chylomicron secretion (48, 49), may be worth future consideration.

Supplementary Material

Refer to Web version on PubMed Central for supplementary material.

ACKNOWLEDGEMENTS

This work was supported by grants HL-38180, DK-56260 (to NOD), DK-112378 (NOD, DR, BWW), HD-083895, HD-065435 (KHM), DK-106382 (DCR) AGA Gilead Research Scholar, Robert Wood Johnson Foundation (BJD), Digestive Disease Research Core Center P30 DK-52574 (Murine models, ARAC, Biobank and a P/F award to BJD), KO8-AI-113184 (ALK), Manpei Suzuki Diabetes Foundation (HM), Diabetes Research Center and the Washington University Metabolomics Facility, supported in part by P30 DK-020579, Nutrition and Obesity Research Center P30 DK-56341.

REFERENCES

1. Collaborators GBDO. Health Effects of Overweight and Obesity in 195 Countries over 25 Years. N Engl J Med. 2017;377(1):13–27. [PubMed: 28604169]
2. Voils CI, Olsen MK, Gierisch JM, McVay MA, Grubber JM, Gaillard L, et al. Maintenance of Weight Loss After Initiation of Nutrition Training: A Randomized Trial. Ann Intern Med. 2017;166(7):463–71. [PubMed: 28241185]
3. Mingrone G, Panunzi S, De Gaetano A, Guidone C, Iaconelli A, Leccesi L, et al. Bariatric surgery versus conventional medical therapy for type 2 diabetes. N Engl J Med. 2012;366(17):1577–85. [PubMed: 22449317]
4. Schauer PR, Kashyap SR, Wolski K, Brethauer SA, Kirwan JP, Pothier CE, et al. Bariatric surgery versus intensive medical therapy in obese patients with diabetes. N Engl J Med. 2012;366(17): 1567–76. [PubMed: 22449319]
5. Cavin JB, Couvelard A, Lebtahi R, Ducroc R, Arapis K, Voitellier E, et al. Differences in Alimentary Glucose Absorption and Intestinal Disposal of Blood Glucose After Roux-en-Y Gastric Bypass vs Sleeve Gastrectomy. Gastroenterology. 2016;150(2):454–64 e9. [PubMed: 26481855]

6. Albaugh VL, Flynn CR, Cai S, Xiao Y, Tamboli RA, and Abumrad NN. Early Increases in Bile Acids Post Roux-en-Y Gastric Bypass Are Driven by Insulin-Sensitizing, Secondary Bile Acids. J Clin Endocrinol Metab. 2015;100(9):E1225–33. [PubMed: 26196952]
7. Flynn CR, Albaugh VL, Cai S, Cheung-Flynn J, Williams PE, Brucker RM, et al. Bile diversion to the distal small intestine has comparable metabolic benefits to bariatric surgery. Nature communications. 2015;6:7715.
8. Ryan KK, Tremaroli V, Clemmensen C, Kovatcheva-Datchary P, Myronovych A, Karns R, et al. FXR is a molecular target for the effects of vertical sleeve gastrectomy. Nature. 2014;509(7499): 183–8. [PubMed: 24670636]
9. Ding L, Sousa KM, Jin L, Dong B, Kim BW, Ramirez R, et al. Vertical sleeve gastrectomy activates GPBAR-1/TGR5 to sustain weight loss, improve fatty liver, and remit insulin resistance in mice. Hepatology. 2016;64(3):760–73. [PubMed: 27312543]
10. Smushkin G, Sathananthan M, Piccinini F, Dalla Man C, Law JH, Cobelli C, et al. The effect of a bile acid sequestrant on glucose metabolism in subjects with type 2 diabetes. Diabetes. 2013;62(4): 1094–101. [PubMed: 23250357]
11. Sugimoto-Kawabata K, Shimada H, Sakai K, Suzuki K, Kelder T, Pieterman EJ, et al. Colestilan decreases weight gain by enhanced NEFA incorporation in biliary lipids and fecal lipid excretion. Journal of lipid research. 2013;54(5):1255–64. [PubMed: 23434610]
12. Pathak P, Xie C, Nichols RG, Ferrell JM, Boehme S, Krausz KW, et al. Intestine farnesoid X receptor agonist and the gut microbiota activate G-protein bile acid receptor-1 signaling to improve metabolism. Hepatology. 2018;68(4):1574–88. [PubMed: 29486523]
13. Arab JP, Karpen SJ, Dawson PA, Arrese M, and Trauner M. Bile acids and nonalcoholic fatty liver disease: Molecular insights and therapeutic perspectives. Hepatology. 2017;65(1):350–62. [PubMed: 27358174]
14. Rao A, Kosters A, Mells JE, Zhang W, Setchell KD, Amanso AM, et al. Inhibition of ileal bile acid uptake protects against nonalcoholic fatty liver disease in high-fat diet-fed mice. Sci Transl Med. 2016;8(357):357ra122.
15. Xie Y, Newberry EP, Young SG, Robine S, Hamilton RL, Wong JS, et al. Compensatory increase in hepatic lipogenesis in mice with conditional intestine-specific Mttp deficiency. The Journal of biological chemistry. 2006;281(7):4075–86. [PubMed: 16354657]
16. Welty FK. Hypobetalipoproteinemia and abetalipoproteinemia. Curr Opin Lipidol. 2014;25(3): 161–8. [PubMed: 24751931]
17. Shen TC, Albenberg L, Bittinger K, Chehoud C, Chen YY, Judge CA, et al. Engineering the gut microbiota to treat hyperammonemia. The Journal of clinical investigation. 2015;125(7):2841–50. [PubMed: 26098218]
18. Zeissig S, Dougan SK, Barral DC, Junker Y, Chen Z, Kaser A, et al. Primary deficiency of microsomal triglyceride transfer protein in human abetalipoproteinemia is associated with loss of CD1 function. The Journal of clinical investigation. 2010;120(8):2889–99. [PubMed: 20592474]
19. La Rosa PS, Warner BB, Zhou Y, Weinstock GM, Sodergren E, Hall-Moore CM, et al. Patterned progression of bacterial populations in the premature infant gut. Proc Natl Acad Sci U S A. 2014;111(34):12522–7. [PubMed: 25114261]
20. Ramnanan CJ, Edgerton DS, Kraft G, and Cherrington AD. Physiologic action of glucagon on liver glucose metabolism. Diabetes Obes Metab. 2011;13 Suppl 1:118–25.
21. Guo S, Copps KD, Dong X, Park S, Cheng Z, Pocai A, et al. The Irs1 branch of the insulin signaling cascade plays a dominant role in hepatic nutrient homeostasis. Mol Cell Biol. 2009;29(18):5070–83. [PubMed: 19596788]
22. Baud G, Raverdy V, Bonner C, Daoudi M, Caiazzo R, and Pattou F. Sodium glucose transport modulation in type 2 diabetes and gastric bypass surgery. Surg Obes Relat Dis. 2016;12(6):1206–12. [PubMed: 27320223]
23. Xie Y, Kennedy S, Sidhu R, Luo J, Ory DS, and Davidson NO. Liver X receptor agonist modulation of cholesterol efflux in mice with intestine-specific deletion of microsomal triglyceride transfer protein. Arteriosclerosis, thrombosis, and vascular biology. 2012;32(7):1624–31.
24. Gonzalez FJ, Jiang C, and Patterson AD. An Intestinal Microbiota-Farnesoid X Receptor Axis Modulates Metabolic Disease. Gastroenterology. 2016;151(5):845–59. [PubMed: 27639801]

25. Prawitt J, Caron S, and Staels B. Glucose-lowering effects of intestinal bile acid sequestration through enhancement of splanchnic glucose utilization. Trends Endocrinol Metab. 2014;25(5): 235–44. [PubMed: 24731596]
26. Haeusler RA, Pratt-Hyatt M, Welch CL, Klaassen CD, and Accili D. Impaired generation of 12-hydroxylated bile acids links hepatic insulin signaling with dyslipidemia. Cell metabolism. 2012;15(1):65–74. [PubMed: 22197325]
27. Repa JJ, Turley SD, Lobaccaro JA, Medina J, Li L, Lustig K, et al. Regulation of absorption and ABC1-mediated efflux of cholesterol by RXR heterodimers. Science. 2000;289(5484):1524–9. [PubMed: 10968783]
28. Vergnes L, Lee JM, Chin RG, Auwerx J, and Reue K. Diet1 functions in the FGF15/19 enterohepatic signaling axis to modulate bile acid and lipid levels. Cell metabolism. 2013;17(6): 916–28. [PubMed: 23747249]
29. Han S, Zhang R, Jain R, Shi H, Zhang L, Zhou G, et al. Circadian control of bile acid synthesis by a KLF15-Fgf15 axis. Nature communications. 2015;6:7231.
30. Hirasawa A, Tsumaya K, Awaji T, Katsuma S, Adachi T, Yamada M, et al. Free fatty acids regulate gut incretin glucagon-like peptide-1 secretion through GPR120. Nat Med. 2005;11(1):90–4. [PubMed: 15619630]
31. Perry RJ, Peng L, Barry NA, Cline GW, Zhang D, Cardone RL, et al. Acetate mediates a microbiome-brain-beta-cell axis to promote metabolic syndrome. Nature. 2016;534(7606):213–7. [PubMed: 27279214]
32. Schroeder BO, and Backhed F. Signals from the gut microbiota to distant organs in physiology and disease. Nat Med. 2016;22(10):1079–89. [PubMed: 27711063]
33. Fang S, Suh JM, Reilly SM, Yu E, Osborn O, Lackey D, et al. Intestinal FXR agonism promotes adipose tissue browning and reduces obesity and insulin resistance. Nat Med. 2015;21(2):159–65. [PubMed: 25559344]
34. Li F, Jiang C, Krausz KW, Li Y, Albert I, Hao H, et al. Microbiome remodelling leads to inhibition of intestinal farnesoid X receptor signalling and decreased obesity. Nature communications. 2013;4:2384.
35. Prawitt J, Abdelkarim M, Stroeve JH, Popescu I, Duez H, Velagapudi VR, et al. Farnesoid X receptor deficiency improves glucose homeostasis in mouse models of obesity. Diabetes. 2011;60(7):1861–71. [PubMed: 21593203]
36. Zhou M, Learned RM, Rossi SJ, Tian H, DePaoli AM, and Ling L. Therapeutic FGF19 promotes HDL biogenesis and transhepatic cholesterol efflux to prevent atherosclerosis. Journal of lipid research. 2019;60(3):550–65. [PubMed: 30679232]
37. de Boer JF, Schonewille M, Boesjes M, Wolters H, Bloks VW, Bos T, et al. Intestinal Farnesoid X Receptor Controls Transintestinal Cholesterol Excretion in Mice. Gastroenterology. 2017;152(5): 1126–38 e6. [PubMed: 28065787]
38. Daniel H, Gholami AM, Berry D, Desmarchelier C, Hahne H, Loh G, et al. High-fat diet alters gut microbiota physiology in mice. The ISME journal. 2014;8(2):295–308. [PubMed: 24030595]
39. Liou AP, Paziuk M, Luevano JM Jr., Machineni S, Turnbaugh PJ, and Kaplan LM. Conserved shifts in the gut microbiota due to gastric bypass reduce host weight and adiposity. Sci Transl Med. 2013;5(178):178ra41.
40. Everard A, Belzer C, Geurts L, Ouwerkerk JP, Druart C, Bindels LB, et al. Cross-talk between Akkermansia muciniphila and intestinal epithelium controls diet-induced obesity. Proc Natl Acad Sci U S A. 2013;110(22):9066–71. [PubMed: 23671105]
41. Plovier H, Everard A, Druart C, Depommier C, Van Hul M, Geurts L, et al. A purified membrane protein from Akkermansia muciniphila or the pasteurized bacterium improves metabolism in obese and diabetic mice. Nat Med. 2017;23(1):107–13. [PubMed: 27892954]
42. Albaugh VL, Banan B, Antoun J, Xiong Y, Guo Y, Ping J, et al. Role of Bile Acids and GLP-1 in Mediating the Metabolic Improvements of Bariatric Surgery. Gastroenterology. 2019;156(4):1041–51 e4. [PubMed: 30445014]
43. Dao MC, Everard A, Aron-Wisnewsky J, Sokolovska N, Prifti E, Verger EO, et al. Akkermansia muciniphila and improved metabolic health during a dietary intervention in obesity: relationship with gut microbiome richness and ecology. Gut. 2016;65(3):426–36. [PubMed: 26100928]

44. Bergheim I, Weber S, Vos M, Kramer S, Volynets V, Kaserouni S, et al. Antibiotics protect against fructose-induced hepatic lipid accumulation in mice: role of endotoxin. J Hepatol. 2008;48(6): 983–92. [PubMed: 18395289]

45. Kaden-Volynets V, Basic M, Neumann U, Pretz D, Rings A, Bleich A, et al. Lack of liver steatosis in germ-free mice following hypercaloric diets. Eur J Nutr. 2018.

46. Spruss A, Kanuri G, Wagnerberger S, Haub S, Bischoff SC, and Bergheim I. Toll-like receptor 4 is involved in the development of fructose-induced hepatic steatosis in mice. Hepatology. 2009;50(4):1094–104. [PubMed: 19637282]

47. Vos MB, and Lavine JE. Dietary fructose in nonalcoholic fatty liver disease. Hepatology. 2013;57(6):2525–31. [PubMed: 23390127]

48. Greuter T, Malhi H, Gores GJ, and Shah VH. Therapeutic opportunities for alcoholic steatohepatitis and nonalcoholic steatohepatitis: exploiting similarities and differences in pathogenesis. JCI Insight. 2017;2(17).

49. Musso G, De Michieli F, Bongiovanni D, Parente R, Framarin L, Leone N, et al. New Pharmacologic Agents That Target Inflammation and Fibrosis in Nonalcoholic Steatohepatitis-Related Kidney Disease. Clin Gastroenterol Hepatol. 2017;15(7):972–85. [PubMed: 27521506]

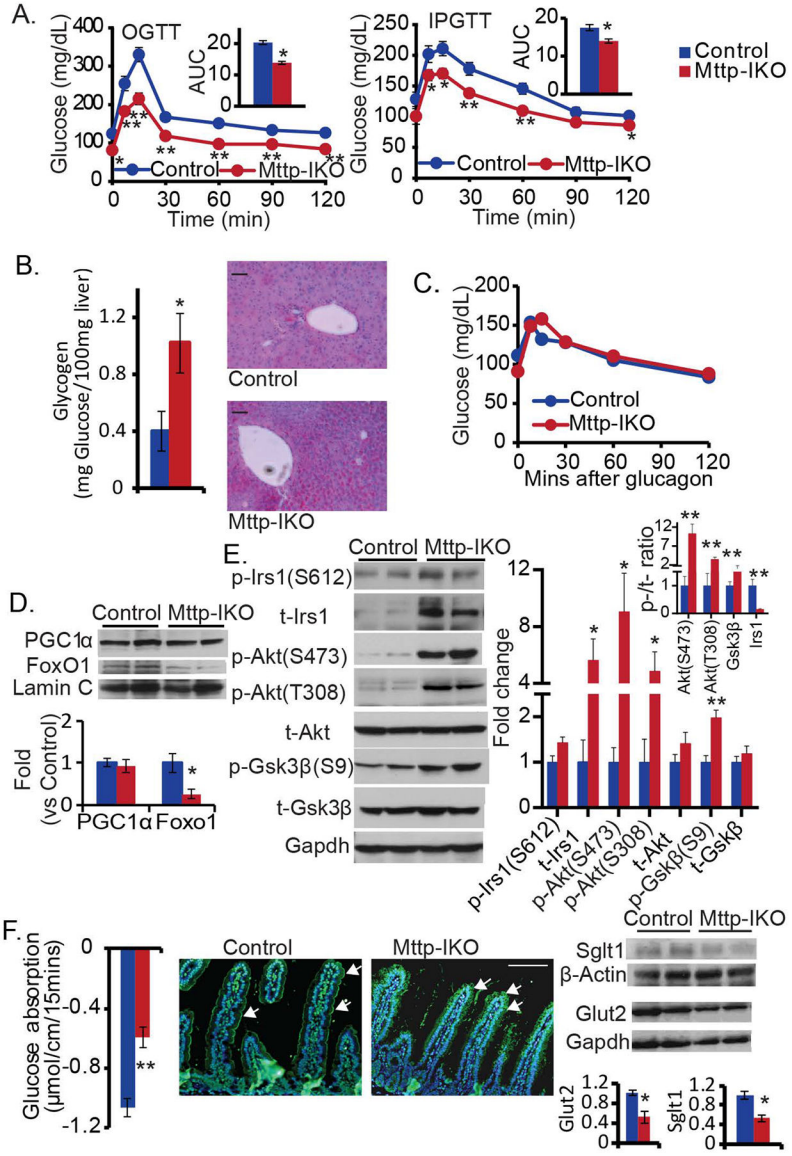

Figure 1. Improved glucose tolerance and hepatic insulin signaling, and decreased intestinal glucose absorption in *Mttp*-IKO mice.

Control and *Mttp-IKO* mice were cohoused. (A) Mice were fasted for 6 hrs, followed by glucose administration either by oral gavage (left) or intraperitoneal injection (right). Plasma glucose was monitored at the indicated time. The major curve graphs represent the plasma glucose excursion; the inserts represent area under curve (AUC). n=8–9 each. OGTT: oral glucose tolerance test. IPGTT: intraperitoneal glucose tolerance test. (B) Livers were harvested after 4 hr fast, hepatic glycogen content was assayed biochemically (left panel) and by periodic acid Schiff (PAS) staining (right panel, Scale bar: 50 μm). n= 8–9 each. (C) Mice were fasted for 6 hr, followed by intraperitoneal injection of glucagon. Plasma glucose was monitored and plotted against the indicated time. n=4 each. (D) Western blot analysis of nuclear expression of PGC1a and FoxO1 protein (Upper). The relative protein abundance was quantitated, after normalization to Lamin C (Lower). n=4–5 each. (E) Hepatic expression of IRS1-Akt-GSK axis (n=4–5 per group) was detected by western blotting. Left

panel: representative images. Right panel: bar graph of densitometric after normalization to GAPDH. (F) Glucose absorption was determined in isolated jejunal loops from control or *Mttp-IKO* mice (right). Representative immunofluorescence images of Sglt1 expression (arrows) in proximal small intestine of control and *Mttp-IKO* mice, with nuclear counterstain (DAPI). Scale bar: 100 micron (middle). Expression of glucose transporters SGLT1 and GlUT2 in small intestinal extracts determined by western blot (right). Upper: representative images, Lower: bar graph of the protein levels of normalized to GAPDH or β-Actin. n=4–5 each. The data are presented as mean ± SEM, *p<0.05, **p<0.01, unpaired t-test.

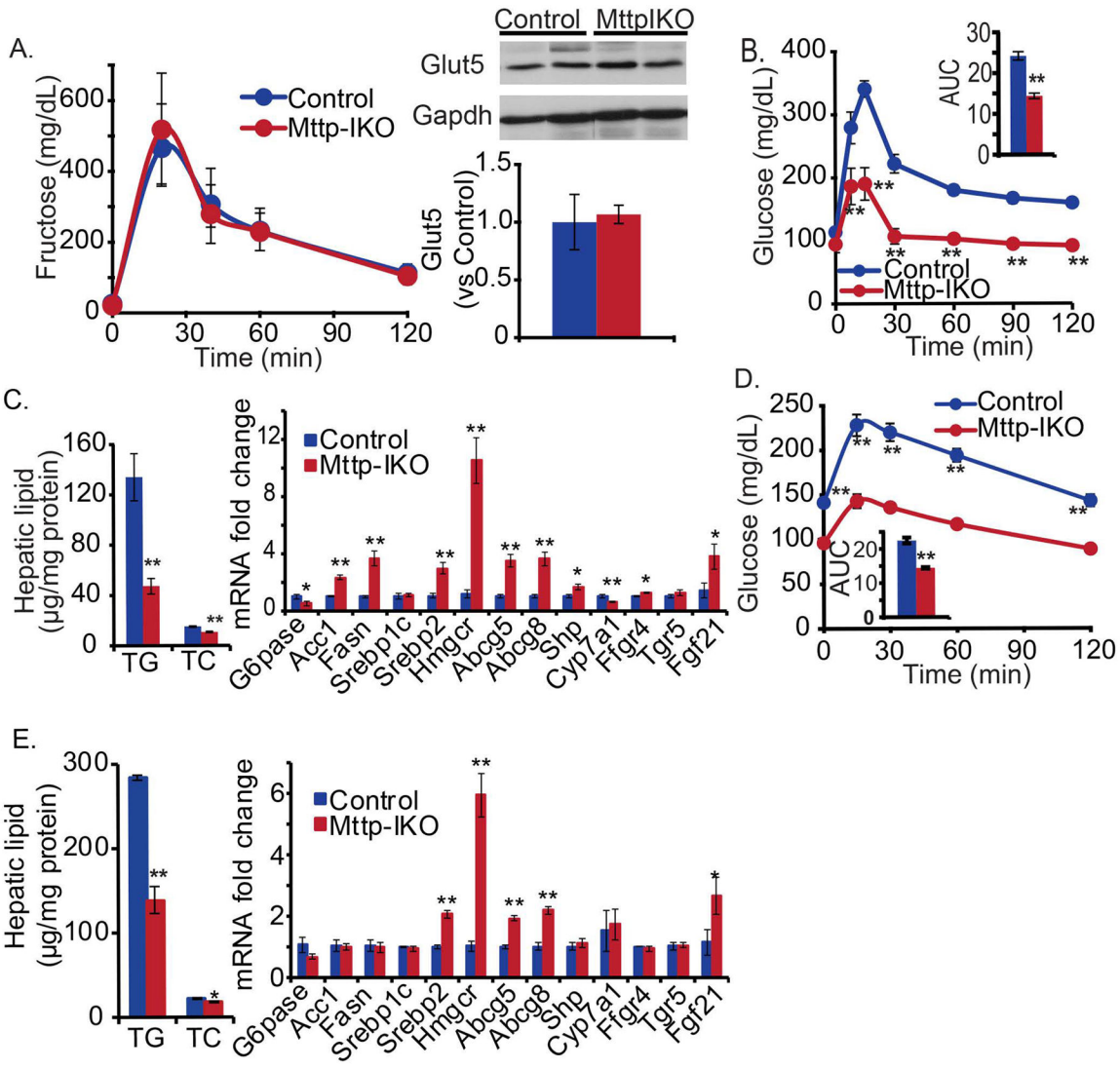

Figure 2. *Mttp*-IKO mice exhibit normal fructose absorption with both protection against and reversal of fructose-induced hepatic steatosis.

Control and *Mttp-IKO* mice were cohoused. (A) Left panel: Mice were fasted for 16 hr, followed by oral gavage of fructose. Serum fructose levels were monitored at the indicated time. n=4 each. Right panel: Intestinal GLUT5 expression by western blot. (B) Oral glucose tolerance tests (OGTTs) were performed on 8–9 mice each after 3 months on high fructose diet; insert panel: area under curve (AUC). (C) Livers were harvested after a 4 hr fast. Hepatic lipids were extracted and determined enzymatically with normalization to protein content (Left). TG: triglyceride, TC: total cholesterol. Hepatic mRNA expression of genes related to lipid metabolism determined by qPCR, normalized to Gapdh (Right). (D) 8 *Mttp* $^{f/f}$ Villin Cre^{ERT2} mice were fed a high fructose for ~18 weeks and a subset (5 of 8) injected with TAM to induce intestinal *Mttp* deletion (*Mttp-IKO*), with another subset (3 of 8) injected with vehicle, as control. Intraperitoneal glucose tolerance tests (IPGTTs) were performed at ~5 weeks following TAM injection. Inset panel: AUC. (E) Hepatic lipids (left)

and hepatic mRNA expression of genes as listed in (C) (right). TG: triglyceride, TC: total cholesterol. The data are mean ± SEM. *p<0.05, **p<0.01. unpaired t-test.

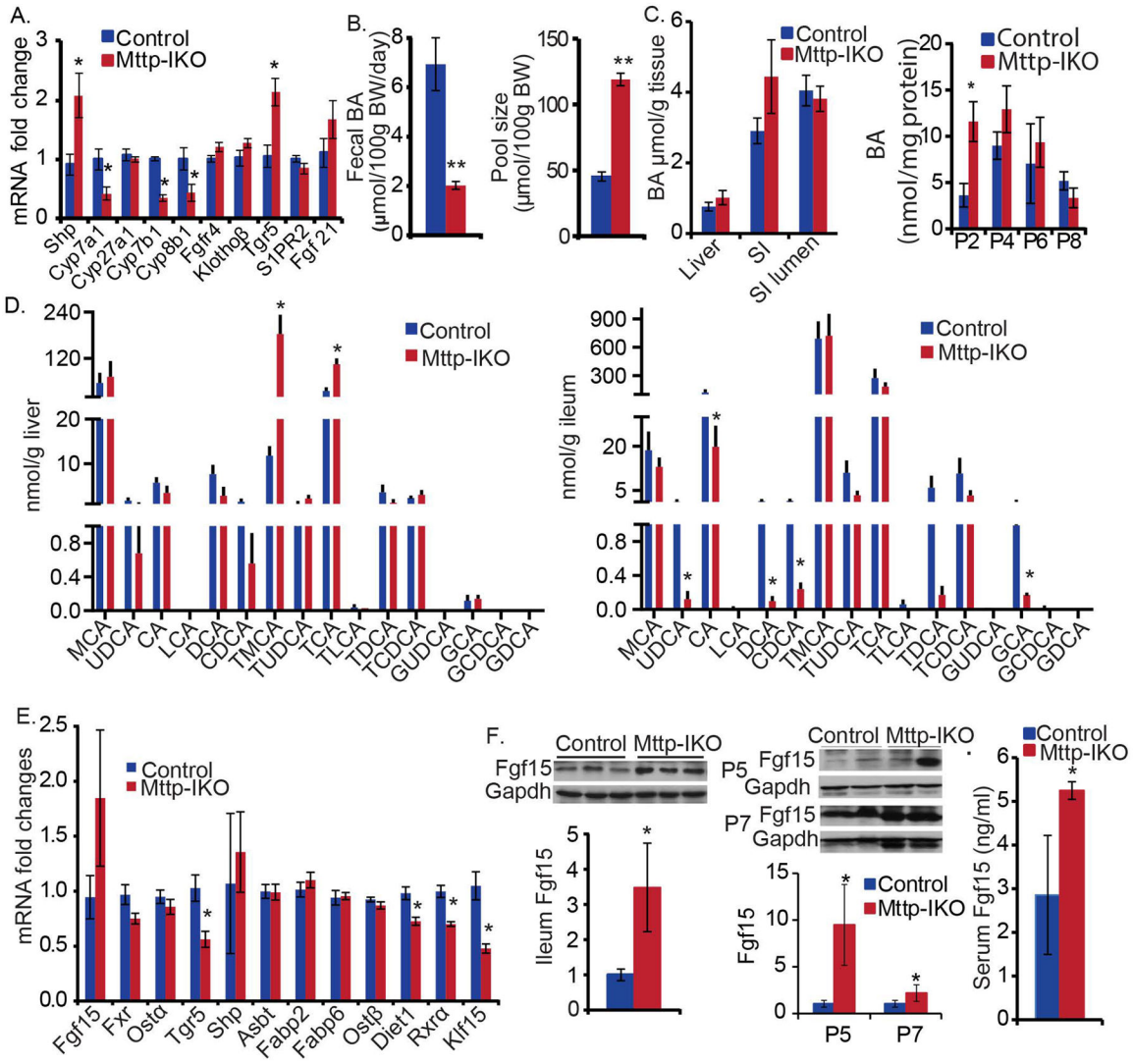

Figure 3. Chow-fed *Mttp*-IKO mice exhibit altered enterohepatic bile acid (BA) content, composition, circulation and pool size with increased intestinal Fgf15 production.

(A) Hepatic mRNA expression of genes related to bile acid (BA) signaling was determined by qPCR. n=8–9 each. (B) and (C) Total BA in tissues was measured enzymatically. (B) Fecal BA excretion was decreased and bile acid pool size was increased in *Mttp-IKO* mice. Mice were individually housed and feces were collected up to 72hr for BA excretion. Liver, gallbladder, and intestine were pooled for BA pool size determinations. (C) Total BA concentration in liver, small intestinal tissue (SI) and small intestinal lumen (SI Lumen), normalized to tissue weight or mg protein. A trend of increased BA in *Mttp-IKO* SI was observed (left). The entire small intestine was equally divided into 8 segments from the duodenum (P1) to ileum (P8) and mucosal extracts used for BA analysis. BA concentration (normalized to protein content) was increased in proximal intestine mucosa of *Mttp-IKO* mice (right). (D) Hepatic (left) and ileal (right) bile acid species were determined by LC-MS/MS. Their concentration was normalized to tissue weight. Identified BA species include muricholic acid (MCA), tauromuricholic acid (TMCA), cholic acid (CA), glycocholic acid (GCA), taurocholic acid (TCA), ursodeoxycholic acid (UDCA), glycoursodeoxycholic acid

(GUDCA), tauroursodeoxycholic acid (TUDCA), lithocholic acid (LCA), taurolithocholic acid (TLCA), chenodeoxycholic acid (CDCA), glycochenodeoxycholic acid (GCDCA), taurochenodeoxycholic acid (TCDCA), deoxycholic acid (DCA), glycodeoxycholic acid (GDCA), taurodeoxycholic acid (TDCA). (E) Ileal mRNA expression of genes related to BA metabolism determined by qPCR. (F) Intestinal and seral FGF15 was increased in *Mttp-IKO* mice. FGF15 protein expression in intestinal segments (divided as the above) was determined by western blotting. Sera were collected at ~6pm after 6hrs-fasting and FGF15 was determined by ELISA. The data in all the bar graphs are presented as mean ± SEM, n=3–5 each, *p<0.05, **p<0.01. unpaired t-test.

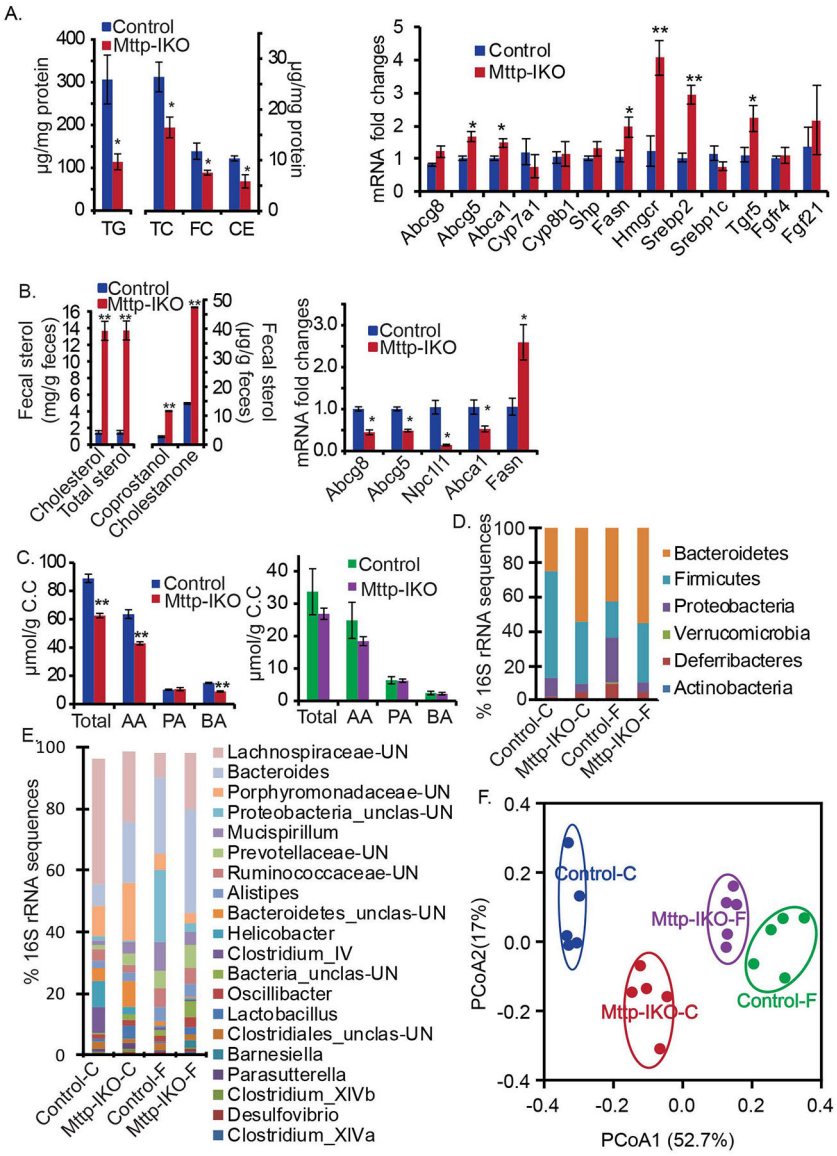

Figure 4. Protection against fructose-induced hepatic steatosis in *Mttp*-IKO mice is associated with increased fecal sterol output and a shift in cecal microbial communities.

Control and *Mttp-IKO* mice were group-housed by genotype and fed 60% fructose diet for 10 days. (A). Hepatic triglyceride (TG), total cholesterol (TC), free cholesterol (FC) and cholesterol ester (CE) content were reduced in Mttp-IKOs (left). n= 10–12 each. Hepatic mRNA expression of genes related to lipid metabolism was determined by qPCR. n=4–10 each (right). (B). Fecal neutral sterols were quantitated by GC (left). n=10–12 each. Expression of intestinal mRNAs was determined by qPCR, n=5 each (right). (C)Cecal contents were extracted and used to determine short chain fatty acid (SCFA) content including acetic (AA), proprionic (PA) and butyric (BA) in mice of the indicated genotype fed either chow (left) or high fructose (right) diets. n= 5 each. The data in (A) to (C) are the mean ± SEM. *p<0.05, **p<0.01. unpaired t-test. Panels (D). (E) and (F). Analysis of gut bacterial communities by 16S rRNA sequencing. n=5 per group. (D). Phylum level changes, showing average percentages of each phylum as a proportion of the whole community, based

on diet and genotype (indicated below X-axis). -C= chow diet; -F= 60% fructose diet for 10 days (E). Genus level changes, showing average percentage of each genus as a proportion of the whole community based on diet and genotype (indicated below X-axis), For simplicity, only genera with relative abundance of >0.1% are displayed. n= 5 per group. Unclas: unclassified, UN: unknown. (F) Principal coordinates analysis of the Bray-Curtis dissimilarity scores is displayed with each dot representing a cecal community from a single mouse. The various diets and genotypes are indicated by color.

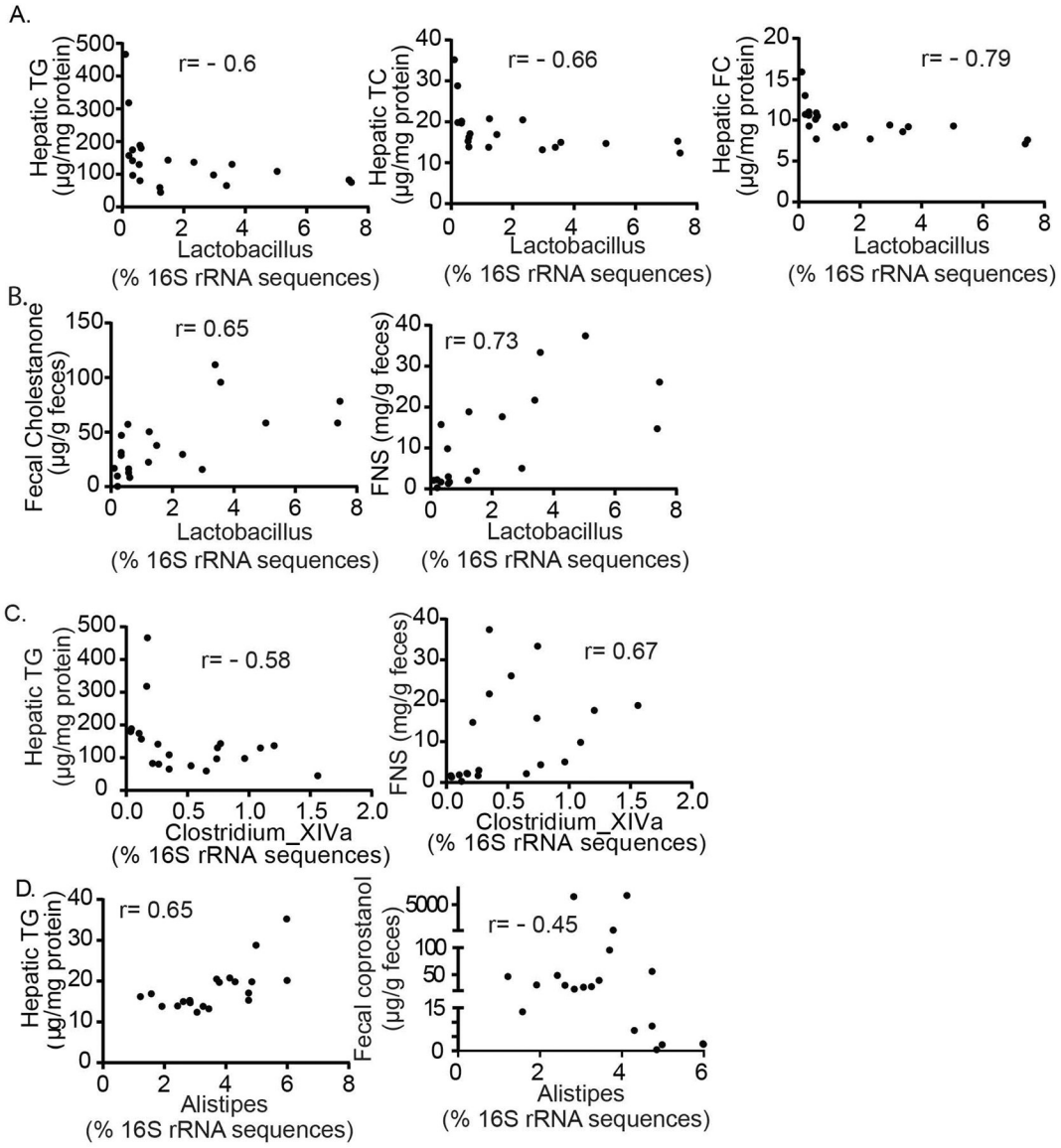

Figure 5. Distinctive patterns of cecal bacterial genus abundance are correlated with either fecal sterol excretion and/or hepatic lipid content.

Pearson-Spearman correlation analysis was used to identify the associated bacteria genus with host hepatic lipid content and/or fecal sterol excretion (Methods). Panel (A) and (B) display that the relative abundance of *Lactobacillus* has an inverse correlation (A) with hepatic TG, TC and FC content and a positive correlation (B) with fecal cholestanone and FNS content. (C) displays that the relative abundance of *Clostridium_XIVa* has an inverse correlation with hepatic TG content, and positive correlation with FNS content. (D) displays that the relative abundance of *Alistipes* has a positive correlation with hepatic TG and inverse correlation with fecal coprostanol. n=20 animals, with coefficient (r) indicted in each graph, $p<0.05$. TG: triglyceride, TC: total cholesterol, FC: free cholesterol, and FNS: fecal neutral sterol.

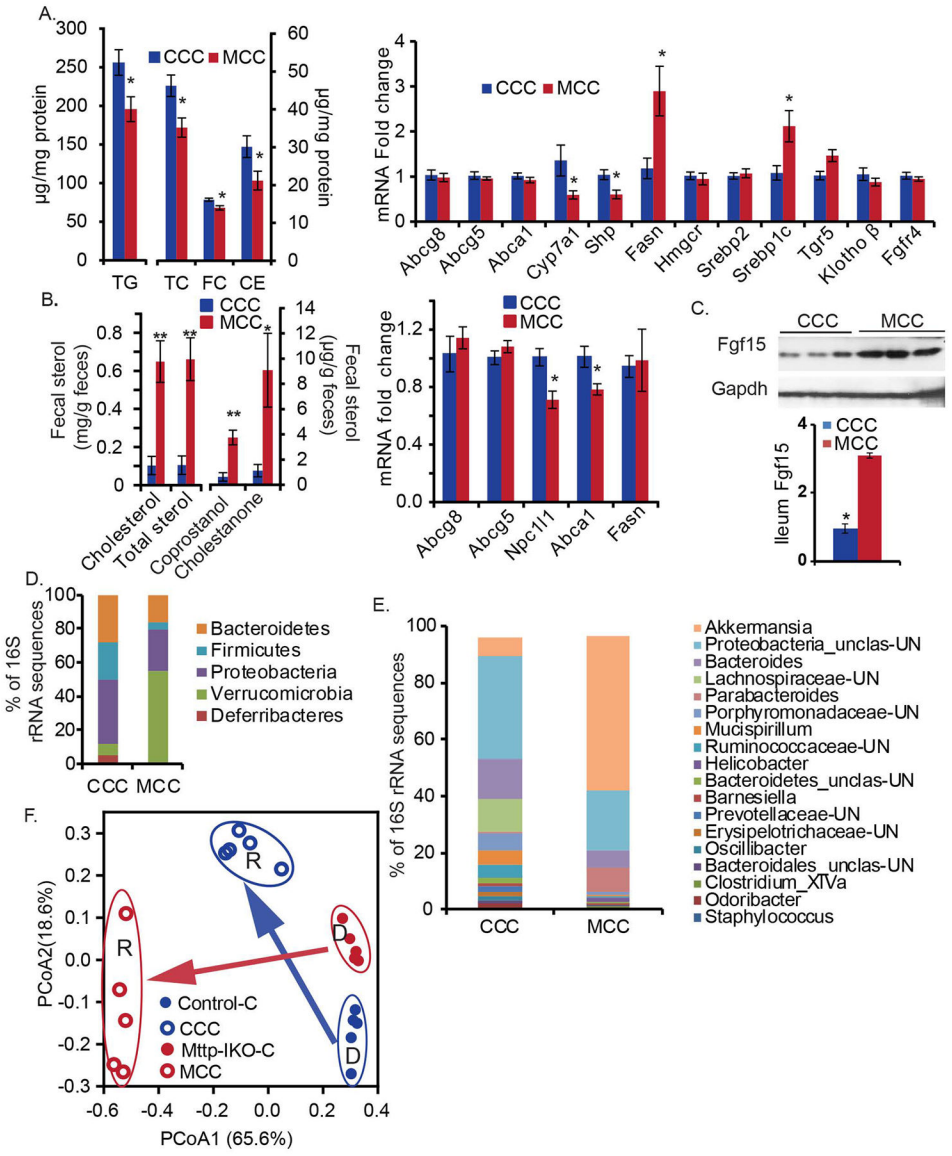

Figure 6. A transmissible phenotype of protection against fructose-induced hepatic steatosis with cecal microbial transplantation (CMT) from *Mttp*-IKO mice.

After treatment with an antibiotic cocktail (Methods), WT recipient mice were cohoused by group, each group receiving pooled donor cecal contents from the indicated genotype, and fed a 60% fructose diet for 10 days. CCC: Chow-fed Control cecal transplant recipient. MCC: Chow-fed *Mttp-IKO* cecal transplant recipient. (A). Hepatic lipids (left panel) were extracted, and assayed, n= 9–10 per group. Hepatic mRNA expression of genes related to lipid metabolism was determined by qPCR (right panel), n=5 per group. (B). Fecal neutral sterol content was determined by GC and normalized to fecal weight, n=5 per group (left). mRNA expression of intestinal cholesterol transporters and fatty acid synthase was determined by qPCR (right), n=5 per group. (C) Ileum Fgf15 was determined by western blot. The data of bar graphs in (A) to (C) are presented as mean ± SEM, unpaired t-test. **p<0.01, *p<0.05. Panels (D), (E) and (F) Analysis of bacterial communities by 16S rRNA gene sequencing from CCC and MCC mice, n=5 per group. (D). Phylum level changes,

showing average percentages of each phylum as a proportion of the whole community, based on genotype of donor cecal content (indicated below X-axis), n= 5 per group. Only phyla with relative abundance >0.5% in at least one sample are displayed. (E) enus level changes, showing average percentage of each genus as a proportion of the whole community based on genotype of donor cecal content (indicated below X-axis. For simplicity, only genera with relative abundance >0.1% are displayed. n= 5 per group. Unclas: unclassified, UN: unknown. (F) Principal coordinates analysis of the Bray-Curtis dissimilarity scores (genus level) is displayed with each dot representing a cecal community from a single mouse. The percentage variation explained by each principal coordinate (PCoA1 and PCoA2) is shown in parentheses. The genotypes of donor cecal content are indicated by color. Solid circles present donors' and empty circles present recipients' microbe communities. R: recipient. D: donor. Arrows: indicated the direction of cecal content transplantation. The microbial communities of recipients clustered together based on the origin of the cecal content received.

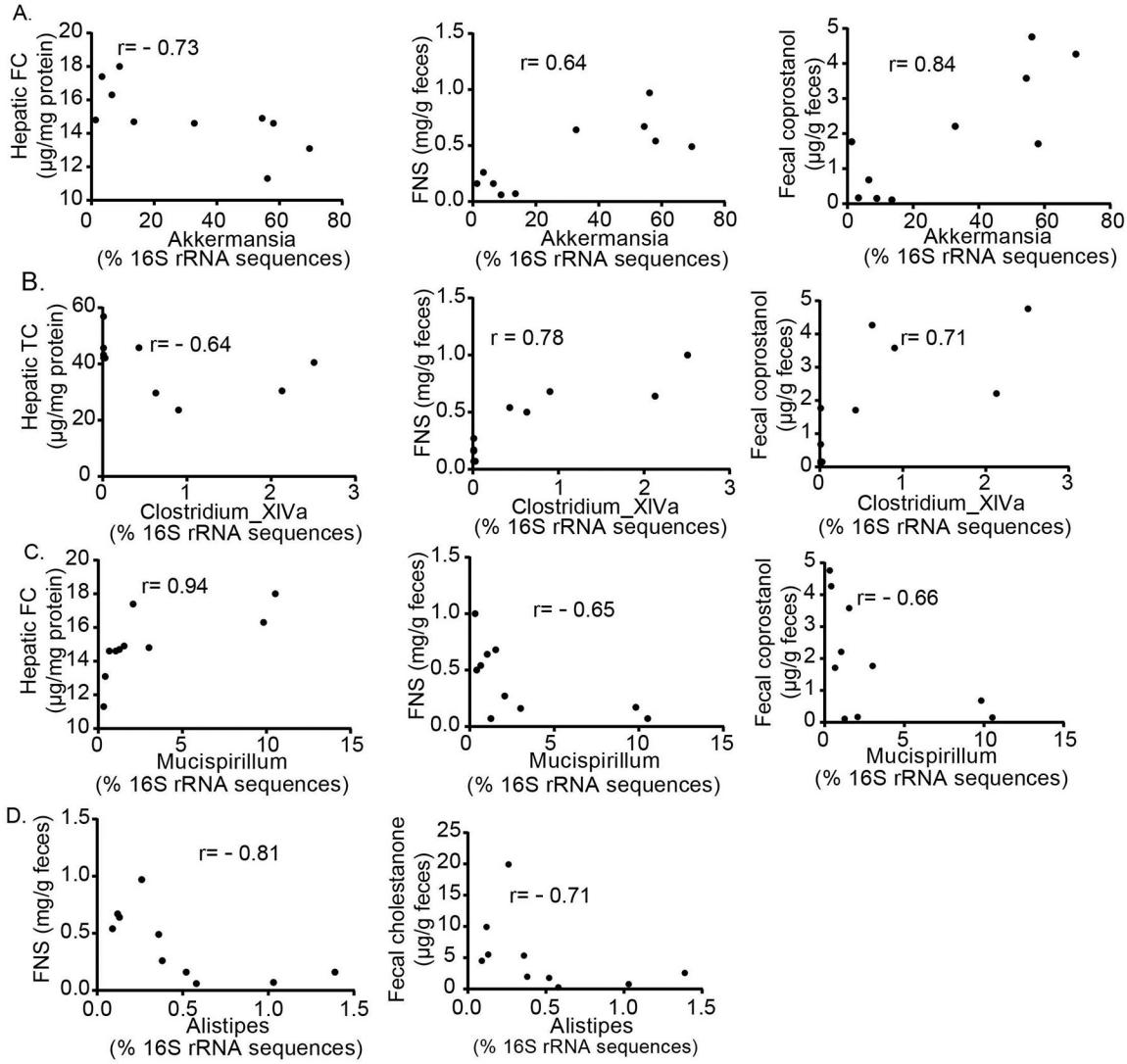

Figure 7. Bacterial genus abundance is correlated with fecal sterol excretion and/or hepatic lipid content following cecal microbial transplantation (CMT) from *Mttp*-IKO mice.

Pearson-Spearman correlation analysis was used to identify the associated bacteria genus with host hepatic lipid content and/or fecal sterol excretion (Methods). (A) demonstrates relative abundance of *Akkermansia* is inversely correlated with host hepatic free cholesterol (FC, left) and positively correlated with fecal neutral sterol (FNS, middle) and fecal coprostanol (right) content. (B) demonstrates relative abundance of *Clostridium_XIVa* is inversely correlated with hepatic total cholesterol (TC), (left), and positively correlated with FNS (middle) and fecal coprostanol (right)content. Panel (C) demonstrates relative abundance of *Mucispirillum* is positively correlated with hepatic FC (left) and inversely correlated with FNS (middle) and fecal coprostanol (right) excretion. (D) demonstrates relative abundance of *Alistipes* is inversely correlated with FNS and fecal cholestanone excretion. n=10 animals, with coefficient (r) indicated in each graph, $p<0.05$.

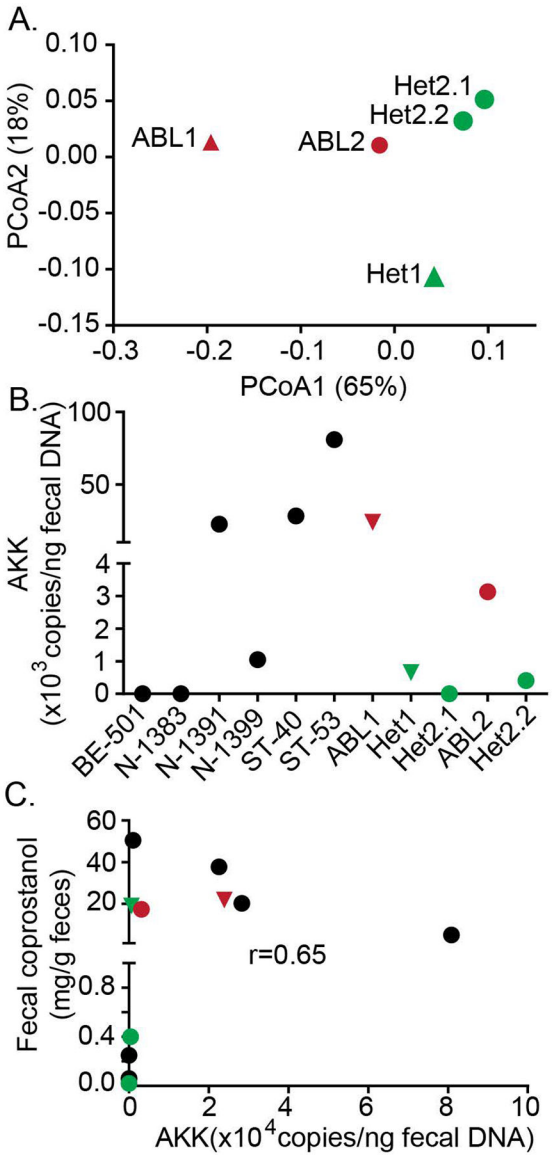

Figure 8. Fecal *Akkermansia* is enriched in Abetalipoproteinemia patients and its abundance is associated with fecal coprostanol in human subjects.

(A) Fecal DNA was extracted from 5 human subjects from two abetalipoproteinemia (ABL) families. Their gut bacterial communities were analyzed by Miseq 16S rRNA gene sequencing (Methods). ABL1 and Het1 were from ABL family 1 (solid triangles). ABL2, Het2.1 and Het2.2 were from ABL family 2 (solid circles). Weighted UniFrac distance was used for principle component analysis. Gut bacterial communities of ABL patients were clustered closer, distinct from their family members. Each dot represents a fecal community. (B) *Akkermansia* abundance in human fecal DNAs (including 6 samples from normal subjects) was determined by qPCR. (C) Fecal neutral sterol content was quantitated by GC (Supplemental Methods). Pearson-Spearman correlation analysis identified a positive correlation between *Akkermansia* abundance and host fecal coprostanol content (right). Red

indicates ABL proband; green indicates the heterozygous family member; black indicates normal controls.